

Multi-Objective Yield Optimization for Electrical Machines using Machine Learning

Morten Christian Huber, Mona Fuhrländer*, Sebastian Schöps

Computational Electromagnetics Group (CEM), Technische Universität Darmstadt, Germany,

*corresponding author's email: mona.fuhrlaender@tu-darmstadt.de

Abstract—This work deals with the design optimization of electrical machines under the consideration of manufacturing uncertainties. In order to efficiently quantify the uncertainty, blackbox machine learning methods are employed. A multi-objective optimization problem is formulated, maximizing simultaneously the reliability, i.e., the yield, and further performance objectives, e.g., the costs. A permanent magnet synchronous machine is modeled and simulated in commercial finite element simulation software. Four approaches for solving the multi-objective optimization problem are described and numerically compared, namely: ε -constraint scalarization, weighted sum scalarization, a multi-start weighted sum approach and a genetic algorithm.

Index Terms—multi-objective optimization, electrical machines, uncertainty quantification, yield, machine learning

I. INTRODUCTION

Electrical machines are increasingly replacing conventional combustion engines, which is an important step against climate change. However, the design and manufacturing process of electrical machines can be further improved to deal responsible with natural resources. Computer simulations, e.g., with finite element method (FEM), have the advantage that products can be virtually analyzed and optimized before the first prototypes are built and tested. This shortens the design process and saves materials. However, typically the simulation of electrical machines is computationally very expensive, since partial differential equations have to be solved numerically, e.g., with FEM. In the approaches we present in this work, these simulations are enabled by the usage of machine learning, more precisely the usage of Gaussian Process Regression (GPR). The proposed workflow considers the FEM simulation tool as a blackbox such that open-source or proprietary software can be used.

Typically, the design, i.e., the geometry and material, of a device is optimized such that performance requirements are fulfilled. However, in practice often there are manufacturing imperfections which lead to deviations in the geometry or material parameters and this may cause violations of the requirements. In this case the manufactured device is rejected. The uncertainty induced by manufacturing uncertainties can be quantified by the yield. The yield describes the probability, that a manufactured device fulfills all performance requirements, under consideration of uncertainties [1].

Classic approaches for yield estimation involve Monte Carlo (MC) analysis [2, Chap. 5]. This sampling-based approach requires the evaluation of the simulation model for each

sample configuration and quickly becomes computationally prohibitive in case of FEM models of electrical machines. Surrogate methods provide an approximation of the quantity of interest (QoI) and proceed a MC analysis on this approximation model, cf. [3]. Examples for surrogates are linear regression [4], stochastic collocation [5] and GPR [6]. However, [7, Example 3.1] shows, that even highly accurate approximation models can lead to wrong yield estimates. For that reason, they introduced a hybrid approach, which evaluates most of the MC sample points on the surrogate model, and a small subset of so-called critical sample points on the high-fidelity model. In [8] a GPR-Hybrid approach has been recently introduced for problems in high-frequency engineering.

In order to improve the reliability of the manufacturing process, the yield shall be maximized. This optimization saves resources, time and money. In practice, besides the reliability, often there are competing objectives, e.g., the minimization of material costs. A multi-objective optimization (MOO) approach is required to find a suitable trade-off between the different objectives. Classic approaches are scalarization methods, e.g., weighted sum [9, Chap. 3] and ε -constraint [9, Chap. 4]. A commonly used heuristic approach are genetic algorithms [10, Chap. 4].

MOO under uncertainty has a long tradition in the design of electric machines [11]. For example, the Taguchi methods, where the loss caused by uncertainty is added to the objective function as penalty term, are popular [12]. Another common approach is worst case optimization [13]. There, the worst case scenario is optimized, i.e., the worst performance of a design considering uncertainties. Since the objective function of the minimization problem is itself a maximization over the uncertainty range, it is a minimax problem [1], [14]. For Gaussian distributed uncertainties, in six sigma design optimization the mean value of the objective function, i.e., the average performance, and the standard deviation (sigma) of the objective function, i.e., the intensity of uncertainty, are minimized, such that the constraints are fulfilled in a six sigma range around the mean value [15]. A recent study comparing these approaches applied to the design of electrical machines is provided in [16]. In the literature, different aspects of electrical machines have been subject to optimization, e.g., the shape of the rotor [17], the permanent magnets (PMs) [18], [19], or the stator slots [20].

In this work a permanent magnet synchronous machine (PMSM) [19] is modeled and simulated using CST Studio

Suite® 2021. Hereby, the size and position of the PMs are considered as deterministic design parameters. The magnitude and the direction of the magnetic fields in the PMs are considered as uncertain design parameters. The average torque is the QoI and equipped with a lower bound it becomes a performance requirement. We apply the GPR-Hybrid approach from [8] to the modeled PMSM in order to achieve efficient and accurate yield estimates. In contrary to [8], the uncertain parameters are not the optimization variables. This becomes especially challenging since closed-form derivatives are not available in this case. We state a MOO problem and provide different formulations for the different optimization methods used, i.e., for weighted sum, ε -constraint and the genetic algorithm. The optimization approaches are applied to the PMSM and evaluated regarding the improvement of the objective functions and their computational efficiency. We propose a multi-start procedure for scalarization methods, which is a heuristic globalization technique. Eventually, we will see that the potentially prohibitive numerical effort can be reduced to an acceptable level by the employed machine learning technique.

The manuscript is structured as follows. We start with an introduction to electrical machines in general and the modeled PMSM in particular in Sec. II. We continue with a section on uncertainty quantification, including the formal definition of the yield and a summary of the GPR-Hybrid approach. In Sec. IV the MOO problem is formulated and the different MOO techniques are introduced. In Sec. V the numerical results are presented, before we conclude with a short summary and an outlook.

II. ELECTRICAL MACHINE SETTINGS

A. Brief introduction to PMSM

As a consequence of the steadily rising focus on mitigating the origins of the climate change and the governments tightening the juridical fundamentals to tackle it, the transport and mobility sector is currently undergoing massive changes with the change from combustion engines to electrical machines. Therefore, it is desired to deploy electrical machines with high power density and great overall efficiency. One machine type that fulfills these requirements is the PMSM. It has several advantages over other machine types such as the induction machine (IM) [21], e.g. increased overall efficiency, reduced size, high power and flux density as well as continuous operation at synchronous speed is possible.

In the PMSM, the rotor consists of PMs that are placed either inside of the rotor design (interior-PMSM) or on the surface of it (surface-PMSM) [21]. The most commonly used elements for the PM are ceramic materials such as Barium Ferrites, rare earth materials such as Samarium and Cobalt or amorphous materials such as Neodymium Iron Boron (NdFeB) which are most often applied in the automotive area [21]. As these resources are considered limited and are subject to significant price volatilities, a minimization of the magnet dimension is desired [22]. The stator, in contrary, is built based on a multiphase symmetrical coil winding (see Figure 1) that is exciting the rotor PMs. As the magnet dimensions of the

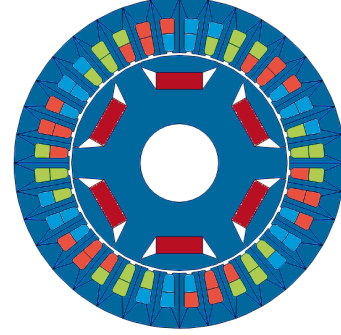


Fig. 1. Design of investigated PMSM containing three polepairs and 36 slots.

PM are considered to be strongly correlating with the machine costs, in this work we will minimize the magnet dimensions and thereby, we minimize the costs of manufacturing the electrical machine. The used PMSM of this paper is based on the benchmark example introduced in [23], where a manufactured PMSM is investigated with regard to a finite element environment.

B. Mathematical foundation

The simulation is carried out based on magnetostatic formulation of Maxwell's equations since the dimensions of the problem are significantly smaller than the wave length. Therefore the displacement current density $\partial\mathbf{D}/\partial t$ is neglected. The resulting equations on a computational domain D are

$$\nabla \times \mathbf{H} = \mathbf{J} + \nabla \times \mathbf{M}, \quad \mathbf{B} = \mu \mathbf{H}, \quad \mathbf{B} = \nabla \times \mathbf{A}, \quad (1)$$

where \mathbf{A} describes the magnetic vector potential, \mathbf{J} the (source) current density, \mathbf{M} the magnetization, μ the permeability, \mathbf{H} the magnetic field strength, \mathbf{B} the magnetic field density. We suppressed spatial and temporal dependencies of the fields for brevity. The equations in (1) can be used to derive the *curl-curl equation* that is the underlying partial differential equation to describe the phenomena of the electrical machine

$$\nabla \times (\nu \nabla \times \mathbf{A}) = \mathbf{J} + \nabla \times \mathbf{M}, \quad (2)$$

where $\nu = \mu^{-1}$ is the magnetic reluctivity. The geometry will be changed during the optimization, i.e., we parametrize the domain $D = D(\mathbf{x})$ using a parameter vector \mathbf{x} . On the other hand, the magnetization $\mathbf{M} := \mathbf{M}(\mathbf{p})$ will depend on uncertainties \mathbf{p} in the magnets. Consequently, the solution $\mathbf{A} := \mathbf{A}(\mathbf{x}, \mathbf{p})$ of (2) inherits those dependencies. Its discretization is carried out by CST Studio Suite® 2021 using higher-order FEM and a domain decomposition approach for the mechanical rotation. We address the solution for some time step t_k by $\mathbf{A}_k(\mathbf{x}, \mathbf{p})$.

C. Assumptions

One of the common drivers for the usage of virtual prototypes is the event of uncertainties during the manufacturing process that influences certain machine performance measurements. These influences on the QoI may lead to a malfunction of the whole machine. These uncertainties are often investigated in a late stage of the product development

under which the efficiency of the whole product lifecycle might suffer. If those uncertainties are included in earlier design stages, more robust design development is possible as the uncertainty propagation can be estimated accurately [19] by means of statistical methods as it will be described in Section III. In the field of electrical machines, there exists a range of parameters that are potentially subject to variations in the manufacturing process [19]. Multiple studies address those parameters, e.g. uncertain material properties due to the welding process, geometrical uncertainties such as rotor eccentricities or variations in the stator slots, and most importantly for the PMSM, uncertainties that are introduced to the geometry and magnetization of the PMs as investigated in [24]–[26]. In [26], it is shown how PMs of three different manufacturers vary in those parameters, i.e., magnitude B_r and direction ϕ of the PM's magnetic field. To investigate their influence, we choose the average torque τ_{avg} over one electrical period

$$t_{\text{ep}} = \frac{1}{n \cdot N_{\text{pp}}} = \frac{60}{1930 \text{ rpm} \cdot 3} \approx 0.01036 \text{ s} = 10.36 \text{ ms}, \quad (3)$$

as the QoI. Here, n describes the speed of the machine in rpm and N_{pp} is the number of pole pairs that are taken from the specifications in Table I. The average torque is calculated as

$$\tau_{\text{avg}} = \frac{1}{N_{\text{per}}} \sum_{k=1}^{N_{\text{per}}} \tau_k, \quad (4)$$

where N_{per} is the number of timesteps used to resolve the electrical period in the transient simulation and $\tau_k := \tau(\mathbf{A}_k)$, $k = 1, \dots, N_{\text{per}}$ the value of the torque in each timestep. All model parameters are given in Table I.

III. UNCERTAINTY QUANTIFICATION

A. Definition of the yield

Let us distinguish between deterministic parameters \mathbf{x} , e.g. the geometry parameters, and uncertain parameters \mathbf{p} , e.g. the magnitude and the orientation of the magnetic field, and one or more QoIs $Q(\mathbf{x}, \mathbf{p})$, e.g. the torque. The uncertain parameters are modeled as random variables. Common modeling choices are the normal or uniform distribution. Following [19], we use the uniform distribution defined by

$$p_i = \bar{p}_i + \Delta p_i \text{ for } i = 1, \dots, n_{\mathbf{p}} \quad (5)$$

with $\Delta p_i \sim \mathcal{U}(-r_i, r_i)$,

where $\mathbf{p} = (p_1, \dots, p_{n_{\mathbf{p}}})^T$, $\bar{p}_i \in \mathbb{R}$ and $r_i > 0$. Let $\text{pdf}(\mathbf{p})$ denote the corresponding multivariate probability density function. We introduce performance feature specifications (pfs) as constraints for the QoI. These are the properties which should be fulfilled by the final design. This is given by

$$Q(\mathbf{x}, \mathbf{p}) \leq c, \quad (6)$$

keeping in mind that in case of several requirements this constraint can be extended. Next, we introduce the safe domain as the set of uncertain parameter combinations fulfilling the pfs, i.e.,

$$\Omega_{\mathbf{x}} := \{\mathbf{p} : Q(\mathbf{x}, \mathbf{p}) \leq c\}. \quad (7)$$

Due to uncertainties in the manufacturing process – represented by the random variables in (5) – it occurs that the manufactured device does not fulfill the pfs, although the nominal design does. Following [1], we can quantify the probability, that the manufactured device fulfills all pfs, by the yield given by

$$Y(\mathbf{x}, \bar{\mathbf{p}}) = \int_{\mathbb{R}^{n_{\mathbf{p}}}} \mathbf{1}_{\Omega_{\mathbf{x}}}(\mathbf{p}) \text{pdf}(\mathbf{p}) d\mathbf{p}, \quad (8)$$

where $\mathbf{1}_{\Omega_{\mathbf{x}}}(\mathbf{p})$ defines the indicator function with value one, if \mathbf{p} lies in $\Omega_{\mathbf{x}}$, and zero otherwise.

B. Estimation of the yield

A straightforward approach in order to estimate the yield is MC analysis [2, Chap. 5]. According to the distribution of the uncertain parameters, a number of N_{MC} sample points $\mathbf{p}^{(1)}, \dots, \mathbf{p}^{(N_{\text{MC}})}$ is generated and then the yield is estimated by

$$Y(\mathbf{x}, \bar{\mathbf{p}}) \approx Y_{\text{MC}}(\mathbf{x}, \bar{\mathbf{p}}) = \frac{1}{N_{\text{MC}}} \sum_{i=1}^{N_{\text{MC}}} \mathbf{1}_{\Omega_{\mathbf{x}}}(\mathbf{p}^{(i)}). \quad (9)$$

The MC analysis is based on the law of large numbers, which is why the standard deviation of the MC estimator depends on the number of MC sample points N_{MC} , i.e.,

$$\sigma_{Y_{\text{MC}}} = \sqrt{\frac{Y(\mathbf{x}, \bar{\mathbf{p}})(1 - Y(\mathbf{x}, \bar{\mathbf{p}}))}{N_{\text{MC}}}} \leq \frac{0.5}{\sqrt{N_{\text{MC}}}}. \quad (10)$$

The inequality in (10) is an upper bound for the worst case scenario when $Y(\mathbf{x}, \bar{\mathbf{p}}) = 0.5$. The $\sigma_{Y_{\text{MC}}}$ serves as measure for the accuracy of the MC estimation and determines the required size of the MC sample set. In the following, we aim to achieve an accuracy of $\sigma_{Y_{\text{MC}}} \leq 0.01$, which leads to a required sample size of $N_{\text{MC}} = 1/(2 \cdot 0.01)^2 = 2500$. Please note, that this sample size is well suited, for yield estimations until 99.9 %, cf. [1, Chap. 4.8.7]. For higher percentages (6-sigma) much higher accuracy is needed, i.e., more sample points or other techniques have to be applied, e.g. importance sampling [27] or subset simulation [28].

In a MC analysis, for each sample point, the QoI has to be evaluated. It follows that the number of sample points required for high accuracy of the MC analysis is prohibitive for the computational effort associated with the finite element (FE) simulations of (1). For this reason, more involved methods have been developed, e.g. importance sampling [27], surrogate modeling [4]–[6] and hybrid approaches, which combine classic MC with surrogate methods [7]. In this work, we extend the GPR-Hybrid approach [8] for efficient yield estimation to electrical machines and integrate it into the pareto optimization framework.

We briefly introduce the main ideas of the GPR-Hybrid approach. GPR is a surrogate technique where the QoI Q is approximated by a Gaussian process. A Gaussian process can be described uniquely by its mean and covariance / kernel function. In this work we choose the mean value of the training data evaluations as mean function and the squared exponential

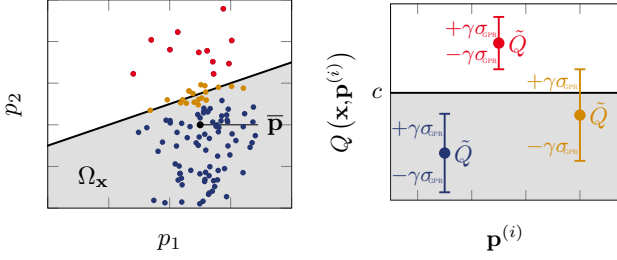


Fig. 2. Visualization of GPR-Hybrid approach with accepted (blue), not accepted (red) and critical (orange) sample points.

kernel (also called radial basis function (RBF) kernel) given by

$$\begin{aligned} \text{cov}(Q(\mathbf{y}), Q(\mathbf{y}')) &= k(\mathbf{y}, \mathbf{y}') \\ &= \zeta^2 \exp\left(-\frac{|\mathbf{y} - \mathbf{y}'|^2}{2l^2}\right), \end{aligned} \quad (11)$$

with the two hyperparameters $\zeta \in \mathbb{R}$ and $l > 0$ and two training data points \mathbf{y} and \mathbf{y}' . Using these assumptions and a set of training data points, a surrogate model of Q is built. Since the surrogate model is a Gaussian process, we can evaluate mean and standard deviation of the surrogate model in any (also unseen) point \mathbf{y}^* . The mean value $\tilde{Q}(\mathbf{y}^*)$ can be used as prediction of the function value $Q(\mathbf{y}^*)$, the standard deviation $\sigma_{\text{GPR}}(\mathbf{y}^*)$ as an error indicator. The availability of an error indicator without additional costs, as well as the possibility of simple model updates due to not requiring structure in the training data set, makes the GPR approach so suitable for hybrid methods. For more detailed information on GPR we refer to [6, Chap. 2].

In the GPR-Hybrid approach, the training data set for the initial GPR surrogate model is chosen small, such that the computational effort is low and the initial accuracy of the GPR model is moderate. The MC analysis is started, i.e., the MC sample set is generated and step by step the sample points are evaluated with the surrogate model. Using a rule based on the prediction and the error indicator, it is decided whether the point is also evaluated on the FE model or not. Then, the sample points are classified as *accepted* (lying inside the safe domain Ω_x) or *not accepted*. Each time, a sample point is evaluated with the FE model, this information is used to update the GPR surrogate model online, i.e., to increase its accuracy, and the remaining sample points are evaluated on the updated surrogate model. In the end, the classification of *accepted* and *not accepted* is used for the yield estimation with (9). The basic procedure is given in Algorithm 1 and a visualization of the classification of the sample points is shown in Fig. 2. In this work, the safety factor is set to $\gamma = 2$. Please note that higher values of the safety factor may increase the number of FE model evaluations, but promise higher accuracy of the yield estimator. For more details we refer to [8].

IV. THE MULTI-OBJECTIVE OPTIMIZATION PROBLEM

A. Formulation of the optimization problem

Having an efficient method for yield estimation, we formulate the optimization problem for the maximization of

Algorithm 1 GPR-Hybrid approach

```

1: Input: MC sample points  $\mathbf{p}^{(i)}$ ,  $i = 1, \dots, N_{\text{MC}}$ , deterministic design point  $\mathbf{x}$ , pfs threshold  $c$ , initial GPR surrogate model  $\tilde{Q}$ ,
2: for  $i = 1, \dots, N_{\text{MC}}$  do
3:   Evaluate the GPR surrogate model and obtain  $\tilde{Q}(\mathbf{x}, \mathbf{p}^{(i)})$  and  $\sigma_{\text{GPR}}(\mathbf{x}, \mathbf{p}^{(i)})$ 
4:   if  $\tilde{Q}(\mathbf{x}, \mathbf{p}^{(i)}) + \gamma\sigma_{\text{GPR}}(\mathbf{x}, \mathbf{p}^{(i)}) \leq c$  then
5:     Classify  $\mathbf{p}^{(i)} \in \Omega_x$  (accepted)
6:   else if  $\tilde{Q}(\mathbf{x}, \mathbf{p}^{(i)}) - \gamma\sigma_{\text{GPR}}(\mathbf{x}, \mathbf{p}^{(i)}) \geq c$  then
7:     Classify  $\mathbf{p}^{(i)} \notin \Omega_x$  (not accepted)
8:   else
9:      $\mathbf{p}^{(i)}$  is a critical sample point
10:    Evaluate the FE model and obtain  $Q(\mathbf{x}, \mathbf{p}^{(i)})$ 
11:    if  $Q(\mathbf{x}, \mathbf{p}^{(i)}) \leq c$  then
12:      Classify  $\mathbf{p}^{(i)} \in \Omega_x$  (accepted)
13:    else
14:      Classify  $\mathbf{p}^{(i)} \notin \Omega_x$  (not accepted)
15:    end if
16:    Update GPR surrogate model  $\tilde{Q}$ 
17:  end if
18: end for

```

the yield, i.e., the maximization of the probability that one realization in a manufacturing process fulfills all performance feature specifications. As optimization variables, the uncertain design parameters can be considered as for example in [29], or both, uncertain and deterministic design parameters can be considered as in [30]. In this work we will focus on deterministic design parameters as optimization variables, i.e., the optimization problem reads

$$\max_{\mathbf{x} \in \mathbb{X}} Y(\mathbf{x}, \bar{\mathbf{p}}), \quad (12)$$

where $\mathbb{X} \subseteq \mathbb{R}^{n_x}$ is the feasible set. In practice, often there is not only the reliability which has to be optimized during the design process, but there are further objectives. This leads to a MOO setting

$$\max_{\mathbf{x} \in \mathbb{X}} f_1(\mathbf{x}, \bar{\mathbf{p}}) \equiv Y(\mathbf{x}, \bar{\mathbf{p}}) \quad (13)$$

$$\max_{\mathbf{x} \in \mathbb{X}} f_i(\mathbf{x}, \bar{\mathbf{p}}), \quad i = 2, \dots, k$$

with k objective functions.

While in single-objective optimization (SOO) the aim is to find the best solution with respect to *one* objective function, in MOO the aim is to find the best solution with respect to *all* objective functions. Since the best solution for the first objective function is, in general, not the best solution for the second objective function, the concept of so-called pareto-optimal solutions have been introduced [9, Def. 2.1]: A feasible solution $\mathbf{x}^* \in \mathbb{X}$ is pareto-optimal, if there is no $\mathbf{x} \in \mathbb{X}$ such that

$$f_i(\mathbf{x}) \geq f_i(\mathbf{x}^*) \text{ for } i = 1, \dots, k \text{ and} \quad (14)$$

$$f_i(\mathbf{x}) > f_i(\mathbf{x}^*) \text{ for some } i \in \{1, \dots, k\}.$$

This implies that a pareto-optimal solution is a solution, such that it is not possible to improve the value of one objective

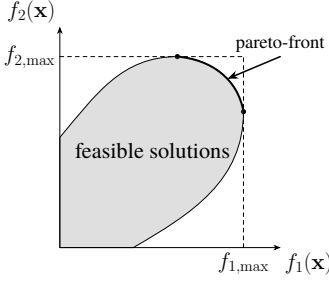


Fig. 3. Visualization of the pareto-front for a bi-objective maximization problem.

function without deteriorating the value of another one. Thus, the solution of a MOO problem is not one single point, but the set of pareto-optimal solutions, the so-called pareto-front. In Fig. 3 the pareto-front of a bi-objective maximization problem is visualized.

B. Scalarization methods

A classic approach for MOO are scalarization techniques like the weighted sum or ε -constraint methods [9, Chap. 3-4]. The basic idea of scalarization is to transform the MOO problem into a SOO problem. In case of the weighted sum scalarization this is achieved by combining all objective functions into one weighted sum which is the new objective function. We obtain

$$\max_{\mathbf{x} \in \mathbb{X}} w_1 Y(\mathbf{x}, \bar{\mathbf{p}}) + \sum_{i=2}^k w_i f_i(\mathbf{x}, \bar{\mathbf{p}}) \quad (15)$$

with weights $w_i > 0$, $i = 1, \dots, k$. In case of the ε -constraint scalarization, only one of the objective functions is maintained, while the remaining objective functions are included into the constraints. This leads for example to the following formulation

$$\begin{aligned} \max_{\mathbf{x} \in \mathbb{X}} Y(\mathbf{x}, \bar{\mathbf{p}}) \\ \text{s.t. } f_i(\mathbf{x}, \bar{\mathbf{p}}) \geq \varepsilon_i, \quad i = 2, \dots, k \end{aligned} \quad (16)$$

with lower bounds $\varepsilon_i \in \mathbb{R}$, $i = 2, \dots, k$. Please note that k different formulations are possible, depending on the choice of the objective function which stays an objective function. The advantage of scalarization techniques is the fact, that after the reformulation we have a SOO problem, which can be solved with classic SOO algorithms like for example simplex algorithms [31] or Sequential Quadratic Programming [32, Chap. 19]. On the other hand, one disadvantage of scalarization is that you obtain only one pareto-optimal solution (not a pareto-optimal front), and this solution depends on the choice of the weights w_i or the bounds ε_i , respectively. Thus, in order to approximate the pareto-front, the reformulated problem has to be solved several times with different values for weights and bounds. Another disadvantage of the weighted sum method is, that convexity requirements on the feasible set \mathbb{X} are required, in order to have the chance to find each pareto-optimal solution. For more details on that we refer to [9, Chap. 3].

Algorithm 2 Multi-start optimization method

- 1: **Input:** set of starting points $\mathbf{x}_0^{(i)}$, i, \dots, N_s , low fidelity model f_L , high fidelity model f_H , optimization problem (P),
- 2: **for** $i = 1, \dots, N_s$ **do**
- 3: Solve (P) based on f_L , starting with $\mathbf{x}_0^{(i)}$ till stopping criterion for exploration phase is reached
- 4: Obtain best solution $\mathbf{x}_*^{(i)}$
- 5: **end for**
- 6: Set $\mathbf{x}_{\text{continue}} = \arg \max_{i=1, \dots, N_s} f_L(\mathbf{x}_*^{(i)})$
- 7: Solve (P) based on f_H , starting with $\mathbf{x}_{\text{continue}}$ till stopping criterion for exploitation phase is reached

C. Multi-start procedure

When using the weighted sum method, we will also investigate a multi-start procedure. By this we try to cover the feasible set best without being trapped in a local optimum. Therefore, a set of starting points is generated and for each starting point the optimization is started. Inspired by the terms of reinforcement learning [33], we refer to this phase as exploration phase, since the aim is to explore as much of the feasible set as possible in order to find the most promising region. After a fixed (not to high) number of objective function evaluations or iterations, the results are compared. Then, the optimization is continued with the solution which had the best objective function value after the exploration phase. This second phase we refer to as the exploitation phase, because now we seek for the best value in this region.

Multi-start procedures are a commonly used heuristic for globalizing local optimization solvers [34, Chap. 6] and appear in many different forms. In its simplest form, several starting points are used, the local optimization is run till the end and then the best solution is chosen. In our setting, each evaluation of the objective function is computationally expensive. Thus, running the local optimization multiple times might be prohibitive. For that reason we establish the two phases and follow only the most promising solution from the exploration phase. The computing time can be further improved, by using lower fidelity models for the exploration phase and a high fidelity model in the exploitation phase. There are many options to distinguish between low and high fidelity models: when using FEM it can refer to the number of elements for example, or in case of yield optimization, it can refer to the size of the MC sample set. The basic procedure is sketched in Algorithm 2.

D. Genetic algorithms

An alternative to scalarization methods are genetic algorithms [10, Chap. 4]. They, in fact, solve MOO problems directly and the solution is an approximation of the pareto-front. Genetic algorithms are motivated by the process of natural evolution of organisms. The basic idea is as follows: a so-called population of individuals, i.e., an initial set of data points, is generated, the objective functions are evaluated on these individuals and in each iteration the population is updated. The update consists of three main elements: selection (survival of the fittest), crossover (reproduction process where

TABLE I
OVERVIEW OVER MOST IMPORTANT MACHINE PARAMETERS [19], [35].

Parameter name	Value
Rotor rated speed n	1930 rpm
Rated current I_{eff}	10.60 A
Average torque (sim.) τ_{avg}	10.64 N m
Windings per coil N_c	12
Stator windings in series a	1
Number of pole pairs N_{pp}	3
Number of slots Q	36
Number of phases m	3
Number of slots per pole and phase q	2
Winding pitch W/τ_p	5/6

genetic traits of the individuals are propagated) and mutation (variation of genetic traits). The rules how these elements are applied, depend on the so-called fitness, a metric for the quality of an individual based on the objective function values.

V. NUMERICAL RESULTS

A. Problem setting

The machine under study is the PMSM from [19], [23] with the properties as specified in Table I. For the uncertainty quantification the deterministic and uncertain parameters need to be concretized. According to measurement studies of a manufactured PMSM in [36], the magnitude $B_{r,i}$ and the direction ϕ_i of the magnetic field of the i -th permanent magnet are consequently assumed uncertain, i.e., they are modeled as uniformly distributed random variables with mean values

$$\bar{\mathbf{p}} = (\bar{B}_{r,1}, \dots, \bar{B}_{r,6}, \bar{\phi}_1, \dots, \bar{\phi}_6) \quad (17)$$

$$= (0.94 \text{ T}, \dots, 0.94 \text{ T}, 0^\circ, \dots, 0^\circ)$$

(see Fig. 4). According to Eq. (5), we write

$$p_i = \bar{p}_i + \Delta p_i \text{ for } i = 1, \dots, 12 \quad (18)$$

with $\Delta p_i \sim \mathcal{U}(-0.05 \text{ T}, 0.05 \text{ T})$ for $i = 1, \dots, 6$

$$\text{and } \Delta p_i \sim \mathcal{U}(-3^\circ, 3^\circ) \text{ for } i = 7, \dots, 12. \quad (19)$$

As the deterministic design parameters we consider the geometric parameters describing the rotor geometry as depicted in Fig. 5, i.e.,

$$\mathbf{x} = (d_1, d_2, d_3, s) \quad (20)$$

$$= (19 \text{ mm}, 7 \text{ mm}, 7 \text{ mm}, 0^\circ).$$

For the mathematical problem formulation of the electrical machine, the magnetostatic simplification of Maxwell's equations (1) is used. The discretization is carried out inside of CST Studio Suite ® 2021 with FEM to acquire a solution for \mathbf{A} in the computational domain (later referred to as FE model). This allows to calculate the QoI, i.e., the average torque τ_{avg}

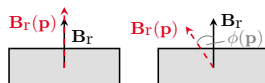


Fig. 4. Geometrical depiction of uncertain rotor design parameters based on [19].

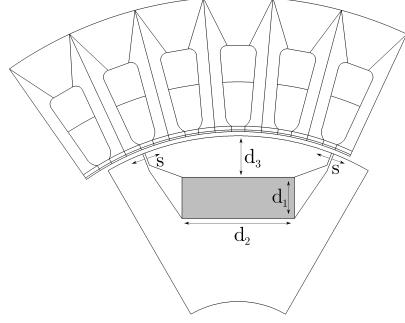


Fig. 5. Geometrical depiction of deterministic motor design parameters \mathbf{x} .

over one electrical period. Next, the QoI is combined with a pfs that includes a lower bound τ_{pfs} for the average torque τ_{avg}

$$Q(\mathbf{x}, \mathbf{p}) := \tau_{\text{avg}}(\mathbf{A}(\mathbf{x}, \mathbf{p})) \geq \tau_{\text{pfs}}. \quad (21)$$

Now we have everything at hand in order to estimate the yield based on (7–8). The general problem formulation for the optimization is based on [19, Eq. (9.52)] and is modified for the purpose of a multi-objective yield and size, i.e., cost, optimization. The modified problem formulation is given by

$$\max_{\mathbf{x} \in \mathbb{R}^4} Y(\mathbf{x}, \bar{\mathbf{p}}) \approx Y_{\text{MC}}(\mathbf{x}, \bar{\mathbf{p}}) = \frac{1}{N_{\text{MC}}} \sum_{i=1}^{N_{\text{MC}}} \mathbf{1}_{\Omega_{\mathbf{x}}}(\mathbf{p}^{(i)}) \quad (22)$$

$$\min_{\mathbf{x} \in \mathbb{R}^4} C(\mathbf{x}) := d_1 d_2 \quad (23)$$

$$\text{s.t. } \mathbf{x} \geq \mathbf{x}_{\text{lb}} \quad (24)$$

$$d_3 \leq d_{3,\text{ub}} \quad (25)$$

$$d_2 + d_3 \leq 15 \quad (26)$$

$$3d_1 - 2d_3 \leq 50 \quad (27)$$

$$s \leq s_{\text{ub}}, \quad (28)$$

where $C(\mathbf{x})$ denotes the additional quantity of the PM surface dimensions that directly correlate with the costs of the PM. As only the surface dimension is varied during the optimization routine and the magnet depth is not considered within the optimization, the surface dimension is mm^2 and consequently considered proportional to the costs.

The stated problem will be tackled with the approaches introduced in Sec. IV. In the applied scalarization methods, the MOO is transformed into a SOO. The SOO framework is built in python using the PDFO framework [37] by M.J.D. Powell that contains optimization methods to efficiently solve SOO problems with linear or nonlinear constraints based on simplex and trust-region methods (see [31], [38], [39] for more details). For the nonlinearly constrained SOO problem COBYLA will be used, which stands for Constrained Optimization By Linear Approximation. The problem formulation including linear constraints will be solved with LINCOA, which stands for Linearly Constrained Optimization Algorithm. Finally, the Genetic Algorithm simulation will be carried out with the pymoo framework of python [40] and uses the NSGA-II algorithm [41].

B. Training of GPR model

In this section the number of training data points for the initial GPR model is derived and the underlying distribution is explained. The two investigated sets of training sample points are drawn from uniform distributions that, first (Case #1), vary in all parameters (features) $\mathbf{x}, \bar{\mathbf{p}}$ and second (Case #2), only in the mean of the uncertain parameters $\bar{\mathbf{p}}$. One should note that the latter case describes the sample point distributions as performed in the later MC analysis to conduct an uncertainty quantification for the initial set of deterministic parameters, whereas the first case describes the process that occurs within the optimization where the deterministic parameters are used as the optimization variables, and, are consequently varied throughout the optimization iterations. The reference yield estimate for $N_{MC} = 2500$ as derived in Sec. III-B that is achieved by solely simulating the MC analysis on the FE model with training sample points as in Case #1 is $Y_{MC}^{(CST)}(\mathbf{x}, \bar{\mathbf{p}}) = 0.0428$. With the MC error indicator from (10) we derive the lower and upper bound of valid yield predictions to use for the validation of the proposed GPR-Hybrid method. We get

$$\sigma_{Y_{MC}} = \sqrt{\frac{Y_{MC}^{(CST)}(\mathbf{x}, \bar{\mathbf{p}})(1 - Y_{MC}^{(CST)}(\mathbf{x}, \bar{\mathbf{p}}))}{N_{MC}}} \approx 0.00405. \quad (29)$$

Consequently, all predictions in the $\sigma_{Y_{MC}}$ region of the yield estimate $Y_{MC}^{(CST)}$, and therefore in $[0.03875, 0.04685]$, are assumed as valid. In the following $\tilde{Y}_{MC}(\mathbf{x}, \bar{\mathbf{p}})$ describes the yield estimation achieved with the GPR-Hybrid method. Table II summarizes the simulation results for the GPR-Hybrid approach for the two proposed cases from above. Here, N_{train} describes the number of training sample points used (offline), N_{online} is the number of re-evaluations on the FE model (online) within the GPR-Hybrid approach, N_{GPR} is the number of evaluations on the GPR model and $N_{train,tot}$ is the sum of offline and online usage of sample points, i.e., $N_{tot} = N_{train} + N_{online}$.

It can be seen that in Case #1 the GPR is capable of delivering very accurate predictions with only 10 initial training data points. The same holds for all considered training set sizes above 10. On the other hand, the GPR built in Case #2, requires a higher number of training data points for accurate predictions – at least 15. The deviations in the yield estimate lie all inside the accepted error tolerance determined

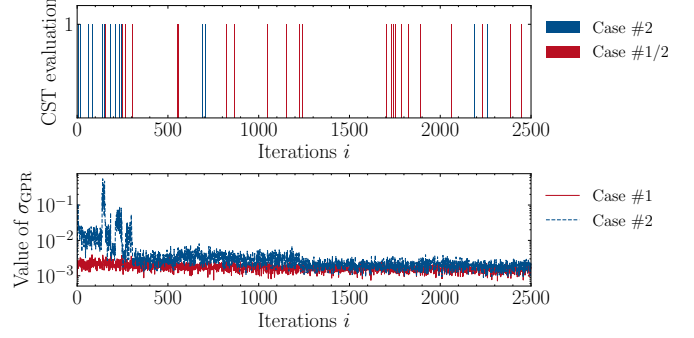


Fig. 6. Comparison of FE model evaluations and GPR standard deviation σ_{GPR} propagation for the two proposed test cases. Iteration i refers to the i -th MC sample point within the GPR-Hybrid approach.

by $N_{MC} = 2500$. It is evident that this prediction performance is a bit worse when compared to Case #1 as the training set does not solely include points that resemble the sample points drawn in a MC analysis, but also the deterministic optimization variables. However, as in the remainder of this paper an optimization over the deterministic parameters is desired, a variation in the deterministic parameters \mathbf{x} is used in the training. Figure 6 shows the iterations in which a re-evaluation on the original model was needed and the correlation to the standard deviation σ_{GPR} of the GPR model prediction. Here, Case #1/2 describes the iterations in which a re-evaluation was needed for both cases. It can be observed that in Case #2 more FE model evaluations are needed in the early stages of the MC analysis that lead to a significant reduction of the standard deviation σ_{GPR} after approximately 250 iterations converging to the value of the standard deviation that was achieved in Case #1. With 20 training data points in Case #2 we have total costs of 60 objective function evaluations and only two sample point differently classified as in the reference solution. In all further experiments we use this size of initial training data points for the optimization. With this, we obtain an approximation not only in the starting point, but in a neighborhood of the starting point. Furthermore, it has to be noted that with the applied GPR-Hybrid approach the number of needed FE model evaluations that take around $t_{FE} = 85$ s is significantly reduced.

C. Optimization results

The parameters of both the ε -constraint and the weighted sum method are varied throughout various optimizations. Additionally, a multi-start procedure is utilized. Finally, a genetic algorithm from the python pymoo package is used and applied to the individual objectives.

1) ε -constraint method: As introduced in Eq. (16), one of the objective functions is transformed into a constraint. The yield function remains objective, while the function of the surface of the PM becomes a constraint, bounded by

TABLE II
OVERVIEW OVER YIELD ESTIMATIONS ACHIEVED WITH THE
GPR-HYBRID APPROACH BASED ON THE TWO PROPOSED CASES OF
TRAINING SAMPLE POINTS.

	N_{train}	$\tilde{Y}_{MC}(\mathbf{x}, \bar{\mathbf{p}})$	N_{online}	N_{GPR}	N_{tot}
Case #1	10	0.0428	26	2474	$10 + 26 = 36$
	20	0.0428	23	2477	$20 + 23 = 43$
	50	0.0428	21	2479	$50 + 21 = 71$
Case #2	15	0.0392	34	2466	$15 + 34 = 49$
	20	0.0436	40	2460	$20 + 40 = 60$
	30	0.0432	43	2457	$30 + 43 = 73$

$\varepsilon \equiv C_{\max}$. The resulting optimization problem reads

$$\begin{aligned} \max_{\mathbf{x} \in \mathbb{R}^4} \quad & Y(\mathbf{x}, \bar{\mathbf{p}}) \\ \text{s.t. } & C(\mathbf{x}) \leq C_{\max} \\ & (24) - (28) \text{ hold.} \end{aligned} \quad (30)$$

As outlined above, the optimization problem is solved with the COBYLA solver of the PDFO framework. The outcome of the simulation can be observed in Table III that shows the chosen bound C_{\max} , the optimized yield estimate $\tilde{Y}_{\text{MC}}^{(\text{opt})}$, the PM surface dimensions of the optimized motor design $C(\mathbf{x})$, the number of objective function calls n_{fev} during the optimization and the number of needed FE model evaluations given as sum of offline and online evaluations. The utilized solver is capable of significantly increasing the yield \tilde{Y}_{MC} for multiple choices of C_{\max} and the resulting surface dimensions are always very close to the upper limit C_{\max} . But it can additionally be observed that if the value of C_{\max} is chosen too low, the optimization routine fails to improve the yield estimate ($C_{\max} = 100$). We see that the choice of $\varepsilon = C_{\max}$ is a trade off between the optimality of the yield and the surface dimensions and is crucial for the result of the optimization, which poses a drawback in practice. The propagation of the yield estimate and the surface dimensions can be seen in Figure 7 and 8. The exploration phase of the simplex methods is observable in the first ten function evaluations as the results for all different settings look comparable in that range. Furthermore, it is evident that the ε -constraint method is varying the design parameters \mathbf{x} such that an improvement of the yield estimate is achieved in a few function evaluations only (e.g., for $C_{\max} = 108$ between the 16th and 18th function evaluation in Figure 7). The same phenomenon is visible in Figure 8 for the PM surface dimensions, where the desired upper boundary for the PM surface dimensions C_{\max} are quickly met. The termination of the algorithm is determined by the applied simplex methods and the correlating trust region subproblem (see [31], [38], [39] for more details).

TABLE III

COMPUTATION STATISTICS OF ε -CONSTRAINT METHOD WITH VARIATION IN C_{\max} .

C_{\max}	$\tilde{Y}_{\text{MC}}^{(\text{opt})}$	$C(\mathbf{x})$	n_{fev}	Total FE evaluations
120	1.0	119.938	17	$20 + 350 = 370$
110	0.998	110.000	35	$20 + 362 = 382$
108	0.996	108.000	42	$20 + 315 = 335$
100	0.0	99.092	38	$20 + 162 = 182$

TABLE IV

COMPUTATION STATISTICS OF WEIGHTED SUM METHOD WITH VARIATION IN THE WEIGHT w .

w	$\tilde{Y}_{\text{MC}}^{(\text{opt})}$	$C(\mathbf{x})$	n_{fev}	Total FE evaluations
1×10^{-3}	0.999	128.963	31	$20 + 259 = 279$
2×10^{-3}	0.996	114.594	35	$20 + 230 = 250$
3×10^{-3}	0.995	109.7022	59	$20 + 262 = 282$
5×10^{-3}	0.978	105.174	100	$20 + 734 = 754$

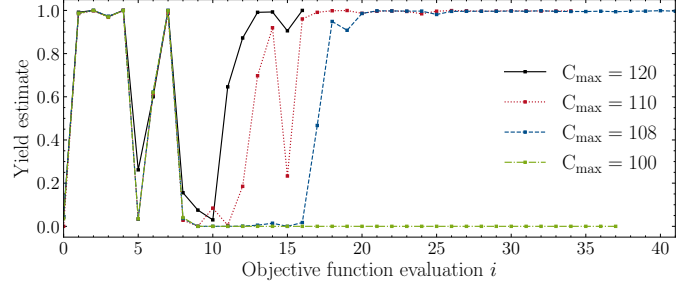


Fig. 7. Propagation of the yield estimate throughout the optimization for the ε -constraint method.

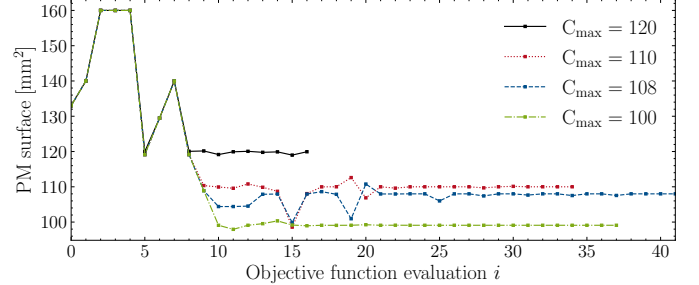


Fig. 8. Propagation of the PM surface dimensions throughout the optimization for the ε -constraint method.

2) *Weighted sum method*: In contrary to the ε -constraint method, the weighted sum method combines both objectives into a weighted sum as in Equation (15) that is consequently minimized. The resulting problem formulation reads

$$\begin{aligned} \min_{\mathbf{x} \in \mathbb{R}^4} \quad & f(\mathbf{x}, \bar{\mathbf{p}}) = -Y(\mathbf{x}, \bar{\mathbf{p}}) + w C(\mathbf{x}) \\ \text{s.t. } & (24) - (28) \text{ hold.} \end{aligned} \quad (31)$$

Therefore, the degree of freedom in that formulation is the weight w that is varied throughout the optimizations conducted with the weighted sum method. The optimization problem is solved with the LINCOA solver of the PDFO framework. The outcome is given in Table IV. The weighted sum approach also proves to significantly increase the yield estimate \tilde{Y}_{MC} of the optimization problem in Eq. (22–28). The weight w is varied from 1×10^{-3} to 5×10^{-3} in four steps. It is evident that the simulation needs more function evaluations when the weight w is increased and, consequently, the surface dimensions $C(\mathbf{x})$ have an increased influence on the objective function (e.g., $n_{\text{fev}} = 31$ for 1×10^{-3} and $n_{\text{fev}} = 100$ for 5×10^{-3}). In the latter case the simulation is terminated because it reached the upper limit of $n_{\text{fev}} = 100$ function evaluations. Similarly to the COBYLA, the LINCOA terminates once the trust region conditions are fulfilled and additionally takes into account the weighted difference of the last four function evaluations given by

$$\Delta_{f_j} = \left| \left(\frac{1}{4} \sum_{i=1}^4 f_{j-i}(\mathbf{x}, \mathbf{p}) \right) - f_j(\mathbf{x}, \mathbf{p}) \right|, \quad (32)$$

where $f_j(\mathbf{x}, \mathbf{p})$ is the objective function value of the j -th function evaluation.

Furthermore, the tradeoff between the surface dimension and the yield estimate is visible in Table IV, as the optimized

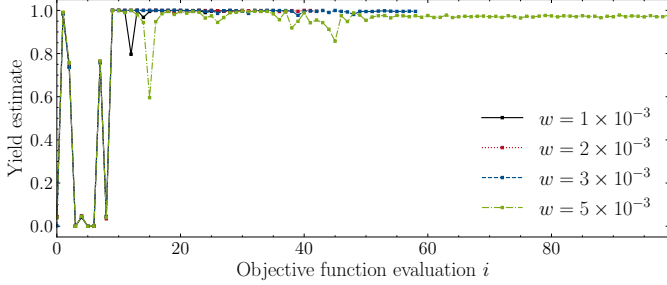


Fig. 9. Propagation of the yield estimate throughout the optimization for the weighted sum method.

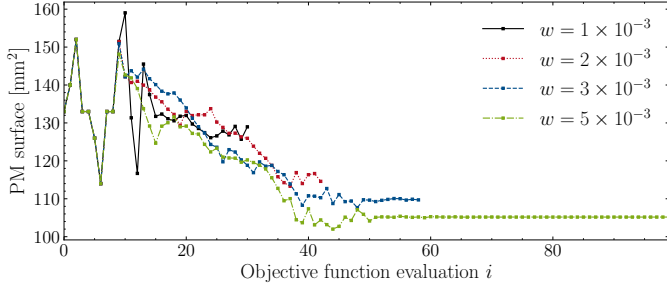


Fig. 10. Propagation of the PM surface dimensions throughout the optimization for the weighted sum method.

yield estimate $\tilde{Y}_{\text{MC}}^{(\text{opt})}$ decreases when the surface dimensions $C(\mathbf{x})$ decreases. The propagation of the yield estimate and the PM surface dimensions is shown in Figure 9 and 10. In comparison to the propagation of the objectives in the ε -constraint method, the optimization needs a larger amount of function evaluations to significantly decrease the surface of the PMs, as there is no target defined for the surface dimensions as with C_{max} in the ε -constraint method.

3) *Multistart procedure*: This section presents the results of the advanced method of including a multistart procedure into the weighted sum optimization to further improve the performance. In general, the two described methods of the ε -constraint and weighted sum method have the disadvantage that a degree of freedom needs to be set, that has a significant influence on the outcome of the optimization as shown in Table III and IV. Especially, the latter has difficulties with nonconvex objectives and is prone to run into suboptimal local minima. Therefore the multistart procedure is applied with the weighted sum method setting that led to higher

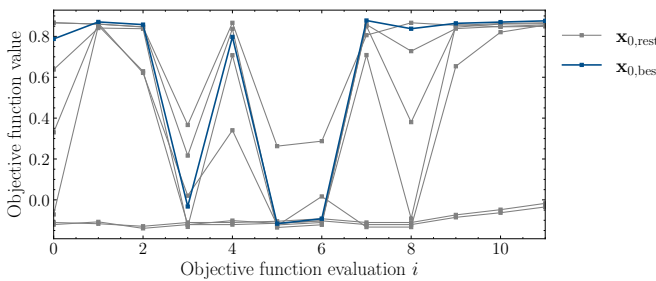


Fig. 11. Demonstration of exploration phase where the best performing starting point is highlighted in blue.

TABLE V
COMPUTATION STATISTICS OF WEIGHTED SUM METHOD WITH AND WITHOUT THE MULTI-START PROCEDURE.

Multi-start	$\tilde{Y}_{\text{MC}}^{(\text{opt})}$	$C(\mathbf{x})$	n_{fev}	Total FE evaluations
no	0.999	128.963	31	20 + 259 = 279
yes	0.998	111.203	135	20 + 394 = 414

surface dimensions of $C(\mathbf{x}) = 128.963 \text{ mm}^2$. The multistart procedure for the first twelve function evaluations with low fidelity, i.e., $N_{\text{MC}} = 100$ can be seen in Figure 11. The starting point $\mathbf{x}_{0,\text{best}}$ represents the design vector \mathbf{x} that led to the best objective value after twelve function evaluations and is highlighted in blue. After the exploration phase with $N_{\text{MC}} = 100$ is completed, the exploitation phase for that starting point is continued with high-fidelity ($N_{\text{MC}}=2500$). The outcome is shown in Table V. We see that by including the multistart procedure, the PM surface dimensions were further decreased by 14 %. This shows, that the disadvantage of scalarization methods to converge into suboptimal local optima can be compensated by the multistart procedure. Furthermore, Figures 12 and 13 show the direct comparison of the weighted sum method with and without the multistart procedure by the propagation of the yield estimate and the PM surface dimensions. It can be seen that the setting of the weighted sum approach without the multistart procedure runs into the local optimum with surface dimensions of 128.963 mm^2 , whereas the application of the multistart procedure leads to a further reduction to $C(\mathbf{d}) = 111.203 \text{ mm}^2$. An exemplary design optimization for the multistart method is shown in Figure 14.

4) *Genetic Algorithm*: This section gives a short outlook into the application of a genetic algorithm applied to the MOO problem. Especially for this kind of computationally expensive problems a fast computation of a single function evaluation is mandatory. With the application of the GPR-Hybrid approach it is possible to reduce the percentage of needed FE model evaluations to approx. 11000, which corresponds to 0.441 % of the total QoI evaluations needed for the genetic algorithm simulation. For the simulation itself we set a budget of 1000 objective function evaluations, i.e., yield estimations, a starting population size of 100 with 50 offsprings in future generations. A snapshot of the resulting pareto front can be seen in Figure

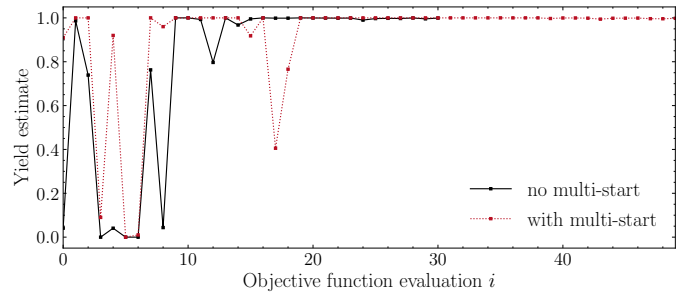


Fig. 12. Comparison of the propagation of the yield estimate throughout the optimization for the weighted sum method with and without the multi-start procedure.

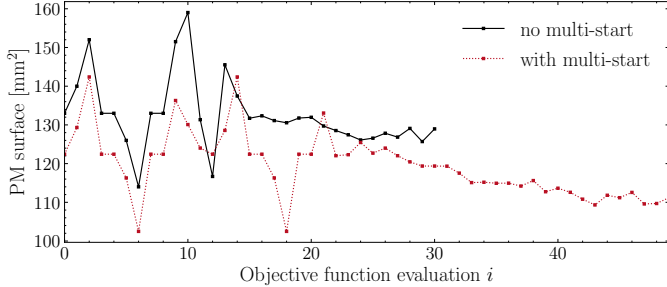


Fig. 13. Comparison of the propagation of the PM surface dimensions throughout the optimization for the weighted sum method with and without the multi-start procedure.

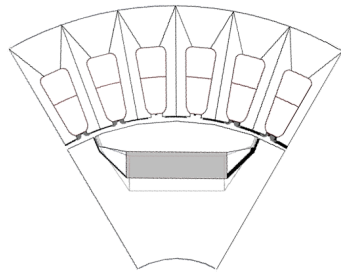


Fig. 14. Optimized design (multi-start method). Here, the filled rectangle displays the optimized design and the contours the original design dimensions.

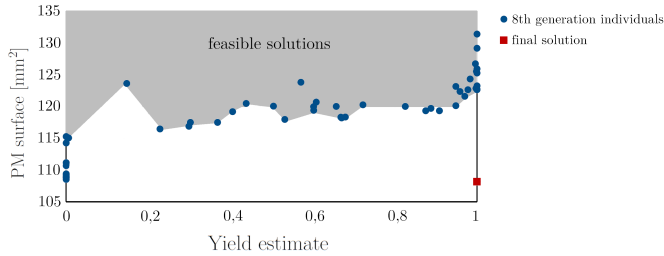


Fig. 15. Visualization of the pareto front of the 8th generation of the genetic algorithm for the stated problem similar to Figure 3. NSGA-II algorithm converges to single solution marked with red square.

15 that displays the individuals of the 8th generation with the feasible solutions depicted in gray. Finally, the NSGA-II algorithm terminates the computation after 1000 function evaluations are conducted and converges to a single point (depicted by the red square in the same figure) with a yield estimate of 1.0 and PM surface dimensions of 108.146 mm². The advantage of the genetic algorithm (GA) simulation is that no further parameters such as a bound C_{\max} or weights w need to be set accordingly to acquire good optima.

VI. CONCLUSION

This paper introduces the application of the GPR-Hybrid method to electrical machines. We show that by using machine learning, the computational effort of yield estimation and yield optimization can be significantly reduced, while maintaining high accuracy. Furthermore, for the design of the electrical machine, multi-objective optimization is applied in order to increase the reliability, i.e., the yield, and to decrease the costs, i.e., the size of the magnets. The scalarization methods

ε -constraint and weighted sum are compared. Both lead to overall high values for the yield estimate, while the rate of decrease of the PM surface dimensions depends on the choice of the scalarization parameters, which is a drawback in practice. On the other hand, the weighted sum method is extended with a multistart procedure that further improves the optimization performance of the utilized methods. Although scalarization parameters still have to be chosen, their impact on the optimization result is greatly reduced. Additionally, a genetic algorithm (GA) is applied, which does not require such a parameter selection. Both methods, GA and weighted sum with multistart procedure, achieve to find a similar optimal solution. The multistart approach requires 4% of the finite element (FE) model evaluations compared to GA.

For future research, however, multiple advanced concepts can be applied. These are, for example, the addition of multiple QoIs for the electrical machine such as the total harmonic distortion, adaptive weight selection for the weighted sum method, or adaptive numbers of the MC sample points.

ACKNOWLEDGMENTS

This work has been supported by the Graduate School CE within the Centre for Computational Engineering at Technische Universität Darmstadt, the Federal Ministry of Education and Research (BMBF) and the state of Hesse as part of the NHR Program and the SFB TRR 361 CREATOR (grant number 492661287) funded by the German Research Foundation DFG.

REFERENCES

- [1] H. E. Graeb, *Analog Design Centering and Sizing*. Dordrecht: Springer, 2007.
- [2] J. M. Hammersley and D. C. Handscomb, *Monte Carlo methods*. Methuen & Co Ltd, 1964.
- [3] C. Bogoclu and D. Roos, “A benchmark of contemporary metamodeling algorithms,” in *ECCOMAS Congress*, Jun. 2016.
- [4] C. R. Rao and H. Toutenburg, *Linear Models: Least Squares and Alternatives*, 2nd ed. New York: Springer, 1999.
- [5] I. Babuška, F. Nobile, and R. Tempone, “A stochastic collocation method for elliptic partial differential equations with random input data,” *SIAM J. Numer. Anal.*, vol. 45, no. 3, pp. 1005–1034, 2007.
- [6] C. E. Rasmussen and C. K. Williams, *Gaussian Processes for Machine Learning*. Cambridge: The MIT Press, 2006.
- [7] J. Li and D. Xiu, “Evaluation of failure probability via surrogate models,” *J. Comput. Phys.*, vol. 229, no. 23, pp. 8966–8980, 2010.
- [8] M. Fuhrländer and S. Schöps, “A blackbox yield estimation workflow with gaussian process regression applied to the design of electromagnetic devices,” *Journal of Mathematics in Industry*, vol. 10, no. 25, 2020.
- [9] M. Ehrgott, *Multicriteria Optimization*. Springer, 2005.
- [10] C. Audet and W. Hare, *Derivative-Free and Blackbox Optimization*, 01 2017.
- [11] P. Di Barba, *Multiobjective Shape Design in Electricity and Magnetism*, ser. Lecture Notes in Electrical Engineering. Springer, 2010.
- [12] G. Taguchi, S. Chowdhury, and Y. Wu, *Taguchi's Quality Engineering Handbook*. John Wiley and Sons, Inc, 2005.
- [13] Z. Bontinck, O. Lass, S. Schöps, H. De Gersem, S. Ulbrich, and O. Rain, “Robust optimization formulations for the design of an electric machine,” *IET Sci. Meas. Tech.*, vol. 12, no. 8, pp. 939–948, 2018-08-13.
- [14] Z. Ren, D. Zhang, and C.-S. Koh, “New reliability-based robust design optimization algorithms for electromagnetic devices utilizing worst case scenario approximation,” *IEEE transactions on magnetics*, vol. 49, no. 5, pp. 2137–2140, 2013.
- [15] S. Xiao, Y. Li, M. Rotaru, and J. K. Sykulski, “Six sigma quality approach to robust optimization,” *IEEE Transactions on Magnetics*, vol. 51, no. 3, pp. 1–4, 2015.

- [16] G. Lei, G. Bramerdorfer, C. Liu, Y. Guo, and J. Zhu, "Robust design optimization of electrical machines: A comparative study and space reduction strategy," *IEEE Transactions on Energy Conversion*, vol. 36, no. 1, pp. 300–313, 2020.
- [17] P. Gangl, S. Amstutz, and U. Langer, "Topology optimization of electric motor using topological derivative for nonlinear magnetostatics," *IEEE Transactions on Magnetics*, vol. 52, no. 3, pp. 1–4, 2015.
- [18] Z. Bontinck, O. Lass, S. Schöps, H. De Gersem, S. Ulbrich, and O. Rain, "Robust optimisation formulations for the design of an electric machine," *IET Science, Measurement & Technology*, vol. 12, no. 8, pp. 939–948, 2018.
- [19] Z. Bontinck, "Simulation and robust optimization for electric devices with uncertainties," Ph.D. dissertation, Technische Universität Darmstadt, 2018.
- [20] M. Arjona, C. Hernandez, and J. Lara, "Electromagnetic optimal design of a permanent magnet synchronous generator," *ICS Newsletter*, vol. 28, no. 3, 2021.
- [21] J. A. Melkebeek, *Electrical Machines and Drives*. Springer International Publishing, 2018.
- [22] J. D. Widmer, R. Martin, and M. Kimiaeigui, "Electric vehicle traction motors without rare earth magnets," *Sustainable Materials and Technologies*, vol. 3, pp. 7–13, 2015.
- [23] U. Pahner, R. Mertens, H. De Gersem, R. Belmans, and K. Hameyer, "A parametric finite element environment tuned for numerical optimization," *IEEE Transactions on Magnetics*, vol. 34, no. 5, pp. 2936–2939, 1998.
- [24] M. A. Khan, I. Husain, R. Islam, and J. Klass, "Design of experiments to address manufacturing tolerances and process variation influencing cogging torque and back emf in the mass production of the permanent magnet synchronous motors," in *Energy Conversion Congress and Exposition (ECCE)*. IEEE, 2012, pp. 3032–3039.
- [25] J. Kolb and K. Hameyer, "Sensitivity analysis of manufacturing tolerances in permanent magnet synchronous machines with stator segmentation," *Transactions on Energy Conversion*, vol. 35, no. 4, pp. 2210–2221, 2020.
- [26] G. Lei, J. Zhu, C. Liu, and B. Ma, "Robust design optimization of electrical machines and drive systems for high quality mass production," in *6th International Electric Drives Production Conference (EDPC)*. IEEE, 2016, pp. 217–223.
- [27] L. Gallimard, "Adaptive reduced basis strategy for rare-event simulations," *Int. J. Numer. Meth. Eng.*, no. 1, pp. 1–20, 2019.
- [28] J. Bect, L. Li, and E. Vazquez, "Bayesian subset simulation," *SIAM/ASA J. UQ*, vol. 5, no. 1, pp. 762–786, Jan. 2017.
- [29] M. Fuhrländer and S. Schöps, "Yield optimization using hybrid gaussian process regression and a genetic multi-objective approach," *Advances in Radio Science*, vol. 19, no. B., pp. 41–48, 2021.
- [30] ——, "Efficient yield optimization with limited gradient information," *arXiv preprint arXiv:2105.07799*, 2021.
- [31] M. Powell, "A view of algorithms for optimization without derivatives," *Centre for Mathematical Sciences, Cambridge University*, 2007.
- [32] M. Ulbrich and S. Ulbrich, *Nichtlineare Optimierung*. Birkhäuser, 2012.
- [33] R. Sutton, *Reinforcement Learning: An Introduction*/Richard S. Sutton, Andrew G. Barto. MIT Press, 1998.
- [34] R. C. Martí, P. M. Pardalos, and M. G. Resende, *Handbook of heuristics*. Springer, 2018.
- [35] U. Pahner, R. Mertens, H. De Gersem, R. Belmans, and K. Hameyer, "A parametric finite element environment tuned for numerical optimization," *IEEE Transactions on Magnetics*, vol. 34, no. 5, pp. 2936–2939, 1998.
- [36] P. Offermann and K. Hameyer, "Stochastic models for the evaluation of magnetisation faults," *COMPEL: The International Journal for Computation and Mathematics in Electrical and Electronic Engineering*, vol. 33, no. 1/2, pp. 245–253, 2013.
- [37] Zhang, Tom M. Ragonneau and Zaikun, "Pdfo - powell's derivative-free optimization solvers," accessed 21.09.2021. [Online]. Available: <https://www.pdfo.net/docs.html>
- [38] M. Powell, "Direct search algorithms for optimization calculations," *Acta Numerica*, Vol. 7, Cambridge University Press, 1998.
- [39] ——, "On fast trust region methods for quadratic models with linear constraints," *Centre for Mathematical Sciences, Cambridge University*, 2014.
- [40] J. Blank and K. Deb, "Pymoo: Multi-objective optimization in python," *IEEE Access*, vol. 8, pp. 89497–89509, 2020.
- [41] K. Deb and H. Jain, "An evolutionary many-objective optimization algorithm using reference-point-based nondominated sorting approach, part i: Solving problems with box constraints," *IEEE Transactions on Evolutionary Computation*, vol. 18, no. 4, pp. 577–601, 2014.